JOURNAL OF MATERIALS SCIENCE 22 (1987) 3765–3770

Cooling rate measurements on pure iron rapidly solidified by piston quenching

F. DUFLOS
Office National d'Etudes et de Recherches Aerospatiales, 92320 Chatillon, France
B. CANTOR
Department of Metallurgy and Science of Materials, University of Oxford, Parks Road, Oxford OX1 3PH, UK

Cooling curves have been monitored during rapid solidification of pure iron, using a rapid response thermocouple embedded in one of the quenching pistons. Cooling rates are found to be typically 10^6 to 10^7 K sec^{-1} in the vicinity of the solidification point at 1500° C, falling to 2×10^4 to 3×10^5 K sec^{-1} at 500° C. Heat-flow analysis shows that cooling conditions during rapid solidification are clearly non-Newtonian, with heat transfer coefficients of 3×10^5 to 6×10^5 W m^{-2} K^{-1} and Nusselt numbers of 0.5 to 1.0. Cooling rates, heat transfer coefficients and Nusselt numbers are higher for piston quenching than for other rapid solidification processes such as melt spinning. Piston-quenched iron microstructures can be ferritic or martensitic depending on the cooling rate during rapid solidification.

1. Introduction

Compared with conventional solidification methods, rapid solidification techniques produce microstructures with refined grain sizes, increased solubility of alloying elements and impurities, reduced levels of segregation, and in some cases the formation of metastable crystalline and amorphous phases [1–3]. In many alloy systems, these effects lead to beneficial improvements in mechanical, magnetic, electrical and other properties. Rapid solidification processing is therefore being used increasingly to manufacture metallurgical materials which take advantage of these improved properties in a variety of applications [1–3].

In all rapid solidification techniques, a mass of liquid metal or alloy is manipulated so as to be thin in at least one dimension, and at the same time in good thermal contact with an efficient heat sink. Under these conditions, heat is extracted quickly from the liquid mass, which then cools and solidifies rapidly. Typical liquid thicknesses are in the range 10 to 100 μm, with corresponding cooling rates in the range 10^5 to 10^6 K sec^{-1}, so that cooling and solidification is usually complete within a few milliseconds [4–7]. Controlling the heat-extraction rate and therefore cooling rate is clearly essential to obtain a reproducible microstructure and maximise the advantages of manufacturing alloys by rapid solidification processing.

Temperatures must be recorded in a very short time interval in order to measure cooling rates during rapid solidification. For this reason, relatively few direct measurements of cooling rate have been reported. Thermoelectric and pyrometric methods have been used to measure cooling rates in the range 10^5 to 10^8 K sec^{-1} during gun and piston quenching [8–15], and photocalorimetric and pyrometric methods have been used to measure similar cooling rates during melt spinning [16–22]. Indirect estimates of cooling rate have also been obtained from the scale of microstructural features such as grain size, dendrite arm spacing, eutectic interphase spacing and dislocation array size [23–27]. However, these indirect estimates are somewhat higher than expected from direct measurements [4–7, 19, 20, 28], and in any case may be unreliable, because microstructure–cooling rate correlations established at low cooling rates must be assumed to remain valid at high cooling rates [4, 19, 20, 28].

The aim of the present paper is to describe direct measurements of cooling rate obtained during piston quenching of pure iron, using a thermoelectric technique in which a rapid-response thermocouple is embedded in one of the quenching pistons. Cooling rates have been measured as a function of liquid superheat and piston velocity, and heat transfer coefficients and Nusselt numbers have been calculated for the piston quenching process using a non-Newtonian heat flow analysis.

2. Experimental procedure

Individual specimens of high-purity iron were rapidly solidified in a piston quenching apparatus which has been described in detail elsewhere [29–31]. Each specimen was r.f. levitation melted in a vacuum chamber which had previously been evacuated and then filled with argon at just below atmospheric pressure. The levitation induction coil was then switched off, so that the molten iron droplet fell under gravity until quenched between two 25 mm diameter polished copper pistons. Each piston was accelerated magnetically by discharging a condenser bank through a coil, which then attracted a mild steel plate attached to the back of the piston. The condenser discharge was triggered photoelectrically by emission of light from the falling

0022–2461/87 $03.00 + .12

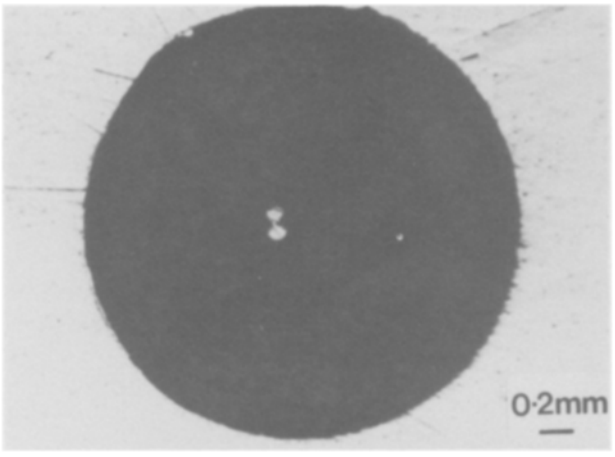

Figure 1 Optical micrograph of rapid response thermocouple junction after polishing.

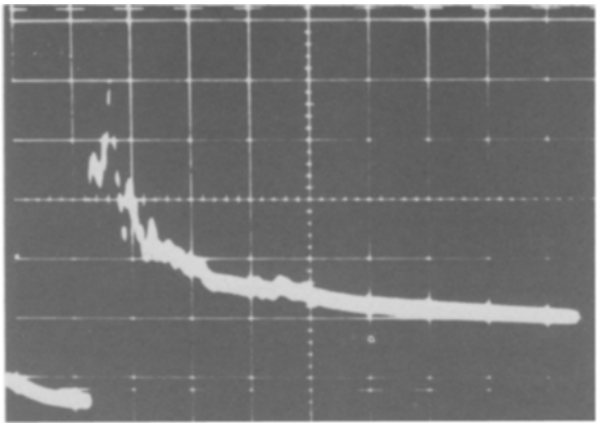

Figure 2 Oscilloscope trace of thermoelectric voltage against time from the rapid response thermocouple during rapid solidification with a piston velocity of 10 m sec^{-1}. Scale divisions are 2 msec and 10 mV.

molten iron droplet. A series of rapid solidification experiments were performed with condenser discharge voltages of 500, 750 and 900 V, corresponding to relative piston closing velocities of 6, 10 and 12 m sec^{-1}, respectively [31]. Two types of iron specimen were used: (a) low superheat specimens of ~ 0.5 g which were r.f. heated for ~ 8 sec and then quenched immediately on melting; and (b) higher superheat specimens of ~ 1.0 g which were r.f. heated for ~ 20 sec prior to quenching. The resulting rapidly solidified iron specimens were in the form of 25 mm diameter discs with typical thicknesses of 50 to 100 μm.

Cooling curves during rapid solidification were measured at the centre of one of the chilled surfaces of each iron disc, using a rapid response chromel/alumel thermocouple embedded in one of the copper pistons. For each rapid solidification run, a fresh thermocouple was manufactured from 90 μm diameter chromel and alumel wires which were spot welded to form a 200 μm diameter junction bead and then set with epoxy resin in a thin-walled alumina insulating tube of 2.7 mm outside diameter. The thermocouple/insulating tube assembly was push-fitted into a 2.7 mm diameter cylindrical hole in one of the copper pistons, and set with epoxy resin so that the junction bead was flush with the piston surface. The junction bead and piston surface were finally polished with 0.3 μm alumina paste until the junction bead was only ~ 25 μm in size. This last step was found to be essential to ensure a sufficiently rapid thermocouple response time. Fig. 1 shows an optical micrograph of a typical embedded thermocouple. During rapid solidification, the thermoelectric signal generated by the rapid response thermocouple was monitored on a cathode ray oscilloscope, which was triggered by a 3 V input from a tension divider across the condenser discharge circuit. Oscilloscope traces were recorded with a polaroid camera.

Surfaces of the rapidly solidified iron discs, and mounted and polished through-thickness cross-sections were etched in 2% nital for metallographic examination in a Cambridge Stereoscan 2A scanning electron microscope. The same specimens were used for microhardness measurements with a Vickers pyramid indentor on a Leitz microhardness tester, using low loads of 25 to 50 g in order to prevent any relaxation effects of the specimen edges. Thin foils of the rapidly solidified iron discs were prepared by window electropolishing in 5% perchloric acid/95% acetic acid at $-60°$ C, 22 V and 2.5×10^3 A m^{-2}, for metallographic examination in a Jeol 120C transmission electron microscope.

3. Results and discussion

Fig. 2 shows a typical oscilloscope trace of thermoelectric voltage against time, obtained from the rapid response thermocouple during rapid solidification with a piston velocity of 10 m sec^{-1}. In general, the oscilloscope traces showed thermocouple response times of 0.3 to 0.5 msec, maximum temperatures of 1300 to 1500° C, and cooling decay times of 1 to 5 msec. The thermocouple tended to pick up noise from electromagnetic fields generated in the accelerating coils and from mechanical vibrations induced during the piston collision. To remove the effects of noise, oscilloscope traces such as in Fig. 2 were smoothed and averaged over several iron specimens rapidly solidified under identical conditions. Some of the resulting cooling curves are shown in Fig. 3 for the

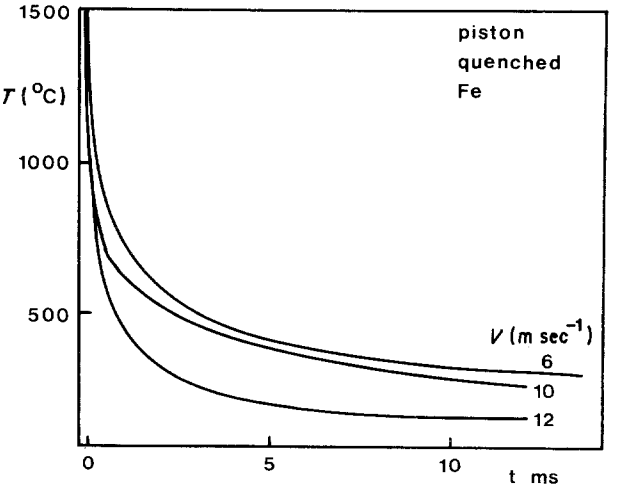

Figure 3 Average cooling curves for low superheat rapidly solidified iron discs with piston velocities of 6, 10 and 12 m sec^{-1}.

TABLE I Average cooling rate as a function of temperature in rapidly solidified iron, measured with a rapid response thermocouple, showing the effects of piston velocity and specimen superheat

Condenser voltage (V)	Specimen mass (g)	Heating time (sec)	Piston velocity ($m\,sec^{-1}$)	Cooling rate ($K\,sec^{-1}$)			
				1500° C	1000° C	750° C	500° C
500	0.5	8	6	4.0×10^6	1.0×10^6	3.0×10^5	8.5×10^4
500	1.0	20	6	4.0×10^6	7.0×10^6	1.5×10^5	4.0×10^4
750	0.5	8	10	9.5×10^6	1.5×10^6	3.5×10^5	9.0×10^4
750	1.0	20	10	1.3×10^6	4.0×10^5	1.4×10^5	6.0×10^4
900	0.5	8	12	1.0×10^7	2.7×10^6	9.0×10^5	2.8×10^5
900	1.0	20	12	4.0×10^6	6.0×10^5	1.2×10^5	2.3×10^4

different piston velocities at low superheat. Table I gives the corresponding cooling rates as a function of temperature. High superheat specimens showed similar cooling curves at all piston velocities, with typical cooling rates of $4 \times 10^6\,K\,sec^{-1}$ at 1500° C falling to $4 \times 10^4\,K\,sec^{-1}$ at 500° C. A similar cooling curve was also found in low superheat specimens rapidly solidified with a piston velocity of $6\,m\,sec^{-1}$. However, cooling rates increased with increasing piston velocity in the low superheat specimens, and were typically $10^7\,K\,sec^{-1}$ at 1500° C and $3 \times 10^5\,K\,sec^{-1}$ at 500° C with a piston velocity of $12\,m\,sec^{-1}$.

Figs 4 and 5 compare the present cooling rate measurements in rapidly solidified iron discs with previous cooling rate measurements in other rapidly solidified metals and alloys. Fig. 4 shows mean cooling rate in the vicinity of the solidification point as a function of piston velocity or melt-spinning wheel velocity, and Fig. 5 shows the same data re-plotted as a function of specimen thickness. (The thickness of melt-spun ribbons is compared with the half-thickness of piston-quenched discs, to allow for the difference between rapid solidification processes with one and two chilled surfaces, respectively.) The cooling rate measurements in Figs 4 and 5 cover a wide variety of different metals and alloys rapidly solidified under a wide variety of different conditions of melt superheat, substrate material, surrounding atmosphere, etc. Measured cooling rates range from 5×10^4 to $2 \times 10^7\,K\,sec^{-1}$ for piston and wheel velocities in the range 1 to $30\,m\,sec^{-1}$ and specimen thicknesses in the range 20 to 130 μm. Within a fair amount of scatter, cooling rates clearly increase with increasing piston or wheel velocity and decreasing specimen thickness.

Under perfect Newtonian cooling conditions, temperature gradients through the thickness of a rapidly solidified iron disc and within the copper pistons are negligible, and the disc temperature, T, decays exponentially with time t [4, 6]:

$$(T - T_p) = (T_s - T_p) \exp(-ht/X\varrho C) \quad (1)$$

where T_p and T_s are initial piston and disc temperatures, and X, ϱ and C are disc half-thickness, density and specific heat, respectively. An equivalent expression can also be obtained for non-Newtonian conditions, allowing for temperature gradients through the disc thickness but neglecting temperature gradients in the piston [4, 32]:

$$(T - T_p) = (T_s - T_p) \times \sum_{m=1}^{\infty} \frac{2N \cos(A_m x/X) \sec(A_m) \exp(-A_m \alpha t/X^2)}{N(N+1) + A_m^2} \quad (2)$$

where the disc temperature, T, is now a function of position x as well as time t, with x measured through

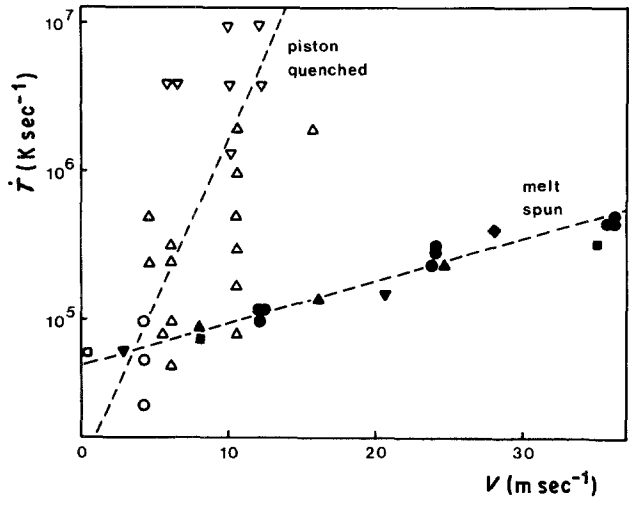

Figure 4 Mean cooling rate in the vicinity of the solidification point, $\dot{T}$, as a function of piston or wheel velocity, V, for a variety of different rapidly solidified metals and alloys [8–12]. Open symbols, piston quenched; closed symbols, melt spun. (●) Ni–5Al, (▲) 316 steel, (■) Cu, (◆) Fe, (▼) nimonic 80A, (▽) Fe, (△) Fe–30Ni, (□) Al, Pb solder, (○) Cu–50Zr, Ni–50Zr.

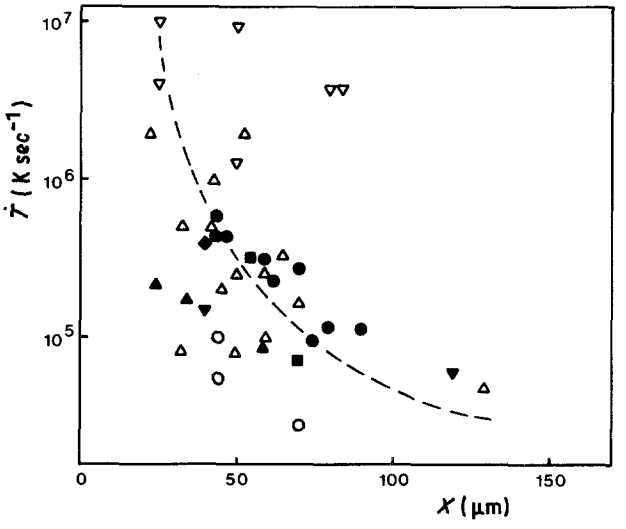

Figure 5 Mean cooling rate in the vicinity of the solidification point, $\dot{T}$, as a function of specimen thickness, X, for a variety of different rapidly solidified metals and alloys [8–12]. Open symbols, piston quenched; full symbols, melt spun (X = half-thickness for piston quenched material). (●) Ni–5Al, (▲) 316 steel, (■) Cu, (◆) Fe, (▼) mimonic 80A, (▽) Fe, (△) Fe–30Ni, (□) Al, Pb solder.

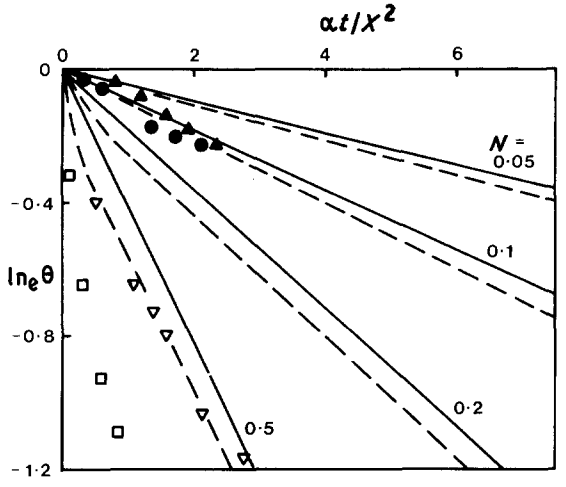

Figure 6 Non-Newtonian heat flow analysis of cooling curves during rapid solidification, plotted as $\ln_e \theta = \ln_e [(T - T_p)/(T_s - T_p)]$ against dimensionless time $\alpha t/X^2$. Calculated lines are from Equation 2 for the centre and chilled surface of a rapidly solidified iron disc. Experimental data points are direct measurements for piston quenched iron at piston velocities of (▽) 10 and (□) 12 m sec^{-1} and melt-spun (●) Ni–5 wt % Al [19] and (▲) 316L stainless steel [20]. (——) θ_0, (– – –) θ_x.

the disc thickness from the disc/piston interface. $N = hX/k$ is the Nusselt number, k and $\alpha = k/\varrho C$ are the disc thermal conductivity and diffusivity, respectively, and A_m is an infinite series of constants obtained from the positive roots of $A \tan A = N$. With electrical noise obscuring any solidification arrest on cooling curves such as in Fig. 2, latent heat of solidification can only be allowed for approximately in Equations 1 and 2 by replacing C with $C + L/\Delta T_s$ where L is latent heat and ΔT_s is solidification range [4, 18, 19]. Finite difference heat flow calculations [33–35] show that there are no significant temperature gradients in the piston when the piston thermal conductivity is greater than the disc thermal conductivity, and no significant temperature gradients in the disc when $N < 10^{-1}$ to 10^{-2}.

Fig. 6 shows data from the cooling curves in Fig. 3, re-plotted in the form $\ln_e [(T - T_p)/(T_s - T_p)]$ against $\alpha t/X^2$ to compare with calculations from Equation 2 for the centre and chilled surface of the piston quenched iron discs ($x = X$ and $x = 0$, respectively) at several Nusselt numbers. Also included in Fig. 6 are previously measured data for melt spun Ni–5 wt % Al [19] and 316L stainless steel [20]. Nusselt numbers in piston quenching are typically 0.5 to 1.0 and cooling conditions are clearly non-Newtonian, whereas Nusselt numbers in melt spinning are typically 0.05 to 0.1, corresponding to near-Newtonian cooling. Heat transfer coefficients calculated from the Nusselt numbers are shown in Fig. 7 as a function of piston or wheel velocity. The heat transfer coefficients are in the range 3×10^5 to 6×10^5 W m^{-2} K^{-1} for piston quenching and 10^4 to 10^5 W m^{-2} K^{-1} for melt spinning. The piston pressure ensures good thermal contact between piston and disc, with correspondingly high values of heat transfer coefficient and Nusselt number for piston quenching compared with melt spinning. As shown in Figs 6 and 7, increasing piston or wheel velocity improves the thermal contact with an increased heat transfer coefficient and Nusselt number.

Figs 8 and 9 show typical scanning and transmission electron micrographs from the rapidly solidified iron discs. The microstructure was either ferritic with a ferrite grain size of 2 to 6 μm and a microhardness of 200 to 250 kg mm^{-2}, or lath martensitic with lath dimensions of 2 to 6 μm long by 0.2 to 0.6 μm wide and a microhardness of 580 to 690 kg mm^{-2}. As shown in Table II, martensite content and therefore microhardness increased with increasing cooling rate during rapid solidification. The microstructure and microhardness of rapidly solidified pure iron is discussed in detail elsewhere [29, 36].

4. Conclusions

Thermoelectric measurements with a rapid response thermocouple during rapid solidification of pure iron by piston quenching show that cooling rates are 10^6 to 10^7 K sec^{-1} in the vicinity of the solidification point at 1500° C, falling to 2×10^4 to 3×10^5 K sec^{-1} at 500° C. Heat-flow analysis of the measured cooling curves shows that cooling conditions are clearly non-Newtonian during rapid solidification by piston

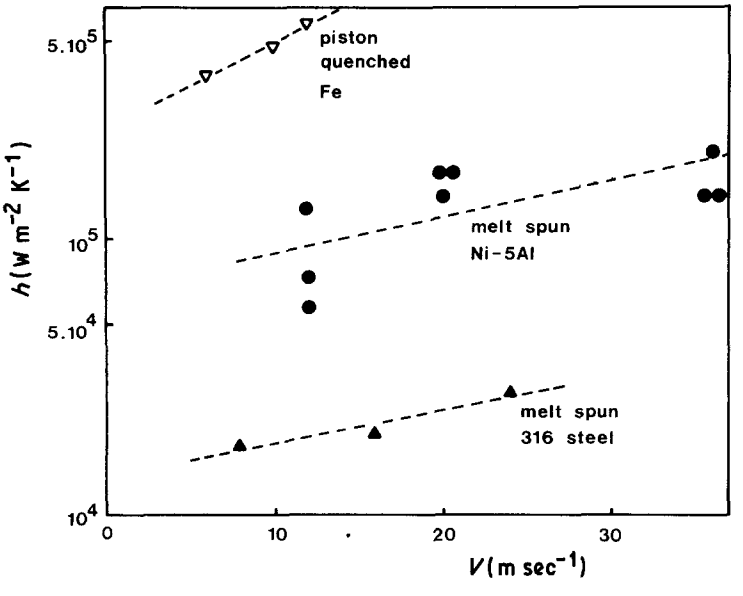

Figure 7 Heat-transfer coefficient as a function of piston or wheel velocity for piston quenched iron and melt-spun Ni–5 wt % Al [19] and 316L stainless steel [20].

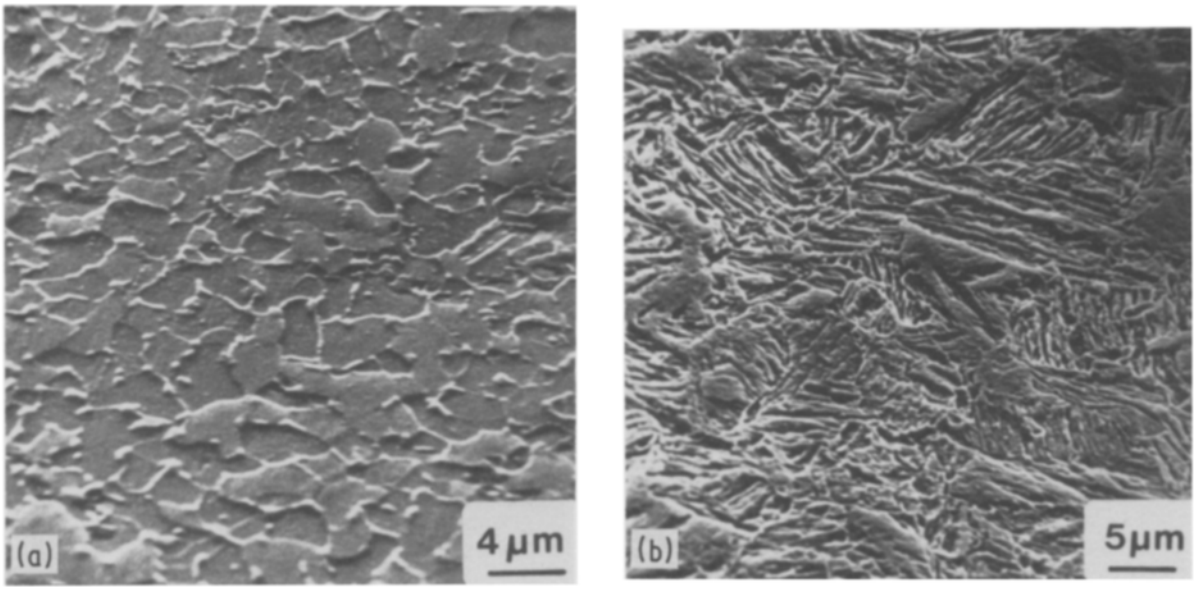

Figure 8 Scanning electron micrographs of rapidly solidified pure iron showing (a) ferritic and (b) martensitic microstructures.

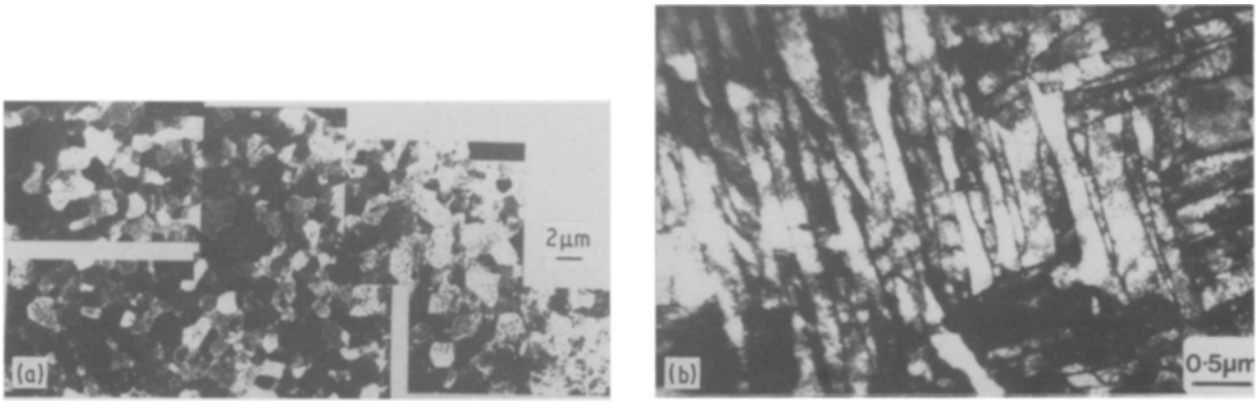

Figure 9 Transmission electron micrographs of rapidly solidified pure iron showing (a) ferritic and (b) martensitic microstructures.

quenching, with heat transfer coefficients of 3×10^5 to 6×10^5 W m^{-2} K^{-1} and Nusselt numbers of 0.5 to 1.0. Cooling rate, heat transfer coefficient and Nusselt number increase with increasing piston velocity and decreasing liquid superheat during rapid solidification. Piston pressure ensures good thermal contact so that cooling rates, heat transfer coefficients and Nusselt numbers are higher for piston quenching than for other rapid solidification processes such as melt spinning. Rapidly solidified pure iron exhibits a ferritic microstructure at low cooling rates and a lath martensitic microstructure at high cooling rates.

TABLE II Microstructure and microhardness of rapidly solidified iron as a function of cooling conditions during rapid solidification

Condenser voltage (V)	Specimen mass (g)	Heating time (sec)	Piston velocity (m sec^{-1})	Cooling rate at 1500° C (K sec^{-1})	Specimen thickness (μm)	Microhardness (kg mm^{-2})	Martensite content (%)	Ferrite grain size/martensite packet size (μm)	Lath dimensions (μm)	
									Length	Width
900	0.5	8	12	10^7	52	690 ± 50	100	3.3	4.0	0.4
					75	580 ± 60	90	3.6	–	0.3–0.5
					87	580 ± 50	90–100	2.4	2.0	0.2
					85	530 ± 30	80	2.4	–	0.3–0.5
900	1.0	8–10	12	–	74	440 ± 10	80	3.5	3.5	0.3–0.5
					62	400 ± 20	60–80	4.5	6.8	0.3–0.5
					93	380 ± 20	40–80	3.7	5.0	0.5
					93	300 ± 10	50–75	3.5	4.0	0.2–0.5
900	1.0	20–25	12	4×10^6	116	300 ± 20	20–60	2.6	–	–
					67	260 ± 10	0	6.0	–	–
					93	260 ± 20	0	3.4	–	–
500	1.0	20–25	6	4×10^6	82	240 ± 10	0	4.0	–	–
					72	230 ± 20	0	5.0	–	–

Acknowledgements

The authors would like to thank Professor R. W. Cahn for provision of laboratory facilities and helpful discussions, and the UK Science and Engineering Research Council, the Centre National de Recherche Scientifique de France and the British Royal Society for financial support of this research.

References

1. B. CANTOR (ed.), "Rapidly Quenched Metals III" (Metals Society, London, 1978).
2. T. MASUMOTO and K. SUZUKI (eds), "Rapidly Quenched Metals IV" (Japan Institute of Metals, Sendai, 1982).
3. S. STEEB and H. WARLIMONT (eds), "Rapidly Quenched Metals V" (North Holland, Amsterdam, 1985).
4. B. CANTOR, in "Science and Technology of the Undercooled Melt", edited by P. R. Sahm, H. Jones and C. M. Adam (Martinus Nijhoff, Dordrecht, 1986) p. 3.
5. *Idem*, in "Rapidly Solidified Amorphous and Crystalline Alloys", edited by B. H. Kear and B. C. Giessen (Elsevier, North Holland, New York, 1982) p. 317.
6. H. JONES, *Rep. Prog. Phys.* **36** (1973) 1425.
7. *Idem*, "Rapid Solidification of Metals and Alloys" (Institution of Metallurgists, London, 1982).
8. P. PREDECKI, A. W. MULLENDORE and N. J. GRANT, *TMS-AIME* **233** (1965) 1581.
9. D. R. HARBUR, J. W. ANDERSON and W. J. MARAMAN, *ibid.* **245** (1969) 1055.
10. I. S. MIROSHNICHENKO and G. P. BREKHARYA, *Phys. Metal Metallogr.* **29** (1970) 233.
11. W. E. BROWER, R. STRACHAN and M. C. FLEMINGS, *Cast Metals Res. J.* **6** (1970) 176.
12. T. Z. KATTAMIS, W. E. BROWER and R. MEHRABIAN, *J. Crystal Growth* **19** (1973) 229.
13. K. LOHBERG and H. MULLER, *Z. Metallkde* **60** (1969) 231.
14. M. NAKA, Y. NISHI and T. MASUMOTO, in "Rapidly Quenched Metals III", Vol. 1, edited by B. Cantor (Metals Society, London, 1978) p. 231.
15. Y. NISHI, T. MOROHOSHI, M. KAWAKAMI, K. SUZUKI and T. MASUMOTO, in "Rapidly Quenched Metals IV", Vol. 1, edited by T. Masumoto and K. Suzuki (Japan Institute of Metals, Sendai, 1982) p. 111.
16. D. H. WARRINGTON, H. A. DAVIES and N. SHOHOJI, *ibid.*, p. 69.
17. M. J. TENWICK and H. A. DAVIES, *ibid.*, p. 67.
18. C. HAYZELDEN, J. J. RAYMENT and B. CANTOR, *Acta Metall.* **31** (1983) 379.
19. A. G. GILLEN and B. CANTOR, *ibid.* **33** (1985) 1813.
20. B. P. BEWLAY and B. CANTOR, *Int. J. Rapid Solidification* **2** (1986) 107.
21. A. J. B. VINCENT, B. P. BEWLAY, B. CANTOR, R. ZABALA, R. P. LaFORCE, S. C. HUANG and L. A. JOHNSON, *J. Mater. Sci. Lett.* **6** (1987) 121.
22. E. VOGT and G. FROMMEYER, in "Rapidly Solidified Materials", edited by P. W. Lee and R. S. Carbonara (ASM, Metals Park, Ohio, 1986) p. 291.
23. P. G. BOSWELL and G. A. CHADWICK, *Scripta Metall.* **11** (1977) 459.
24. H. MATYJA, B. C. GIESSEN and N. J. GRANT, *J. Inst. Metals* **96** (1968) 30.
25. J. V. WOOD and K. N. AKHURST, *J. Mater. Sci.* **11** (1976) 2142.
26. M. H. BURDEN and H. JONES, *Metallogr.* **3** (1970) 307.
27. J. V. WOOD and R. W. K. HONEYCOMBE, *J. Mater. Sci.* **9** (1974) 1183.
28. B. P. BEWLAY, A. G. GILLEN and B. CANTOR, to be published.
29. F. DUFLOS and B. CANTOR, *Acta Metall.* **30** (1982) 323.
30. Y. INOKUTI and B. CANTOR, *ibid.* **30** (1982) 343.
31. R. W. CAHN, K. D. KRISHNANAND, M. LARIDJANI, M. GREEHOLZ and R. HILL, in "Rapidly Quenched Metals II", Vol. II, edited by N. J. Grant and B. C. Giessen (Elsevier North Holland, Lausanne, 1976) p. 83.
32. H. S. CARSLAW and J. C. JAEGER, "Conduction of Heat in Solids" (OUP, Oxford, 1959).
33. R. C. RUHL, *Mater. Sci. Engng* **1** (1967) 313.
34. C. HAYZELDEN, DPhil thesis, Sussex University (1984).
35. T. W. CLYNE, *Met. Trans.* **15B** (1984) 369.
36. F. DUFLOS and B. CANTOR, in "Rapidly Quenched Metals III", Vol. I, edited by B. Cantor (Metals Society, London, 1978) p. 110.

Received 28 November 1986
and accepted 29 January 1987